



Structural damage identification based on estimated additional virtual masses and Bayesian theory

Zhenkun Li¹ · Jilin Hou¹ · Łukasz Jankowski²

Received: 18 August 2021 / Revised: 13 December 2021 / Accepted: 15 December 2021
© The Author(s), under exclusive licence to Springer-Verlag GmbH Germany, part of Springer Nature 2022

Abstract

A novel criterion, based on additional virtual masses estimated in multiple tests and the Bayesian theory, is proposed in this paper to improve the efficiency and precision of damage identification. Initially, a method is proposed that uses the experimentally measured frequency-domain response and a predetermined target frequency to estimate the required additional virtual mass. The proposed mass estimation method is flexible with respect to the frequency band of excitation, which can be thus selected according to practical engineering constraints. Furthermore, a new objective function based on the residual between the theoretical and experimental virtual masses is proposed. The objective function avoids calculating the structural modes through Eigen decomposition of the structural mass and stiffness matrices, and it thus improves the computational efficiency. Thirdly, based on the theoretical frequency response function of the finite element model, explicit formulas are derived for quick calculation of the additional masses and their sensitivities with respect to damage factors. In the next step, randomness and the influence of measurement noise are considered, and the approach is formulated in the probabilistic Bayesian framework. Finally, numerical simulations of a simply supported beam, a 3D truss structure and a 3D building, as well as an experimental 3-story frame, are used to verify the effectiveness of the proposed methods. The results clearly indicate that identified damage factors are close to real values, and thus acceptable in engineering.

Keywords Structural health monitoring (SHM) · Damage identification · Additional virtual mass · Sensitivity analysis · Bayesian theory

1 Introduction

The number, scale, and complexity of civil engineering structures are increasing, and their failures can have fatal outcomes. Damage identification, one of the most important branches of structural health monitoring (SHM), can lay theoretical foundations for monitoring, early warning, and safety assessment of civil structures (Jayalakshmi and Rao 2017). Dynamics-based damage identification methods, due

to their convenient application in practical engineering, can contribute to this goal.

Structural dynamic responses contain ample information about structural health conditions, so that signal processing methods can be used to directly provide information about structural damages. These methods often rely on wavelet transform, empirical mode decomposition (EMD), Hilbert–Huang transform (HHT), and variational mode decomposition (VMD) (Bayissa et al. 2008; Dragomiretskiy and Zosso 2014; Bagheri et al. 2018; Moughty and Casas 2018; Lazhari and Sadhu 2019; Spanos et al. 2020). Such approaches do not need to process FE models of the monitored structures and thus they can quickly identify damages. However, signal processing methods tend to detect just the position of the damage, but not its precise degree. The task of accurate quantification of the position and degree of the damage requires a FE model of the structure to be involved, and structural time-domain responses can be a good reference for such damage identification. It usually involves methods that intensively process structural equations of

Responsible Editor: Byeng D. Youn

✉ Jilin Hou
houjilin@dlut.edu.cn

¹ School of Civil Engineering, State Key Laboratory of Coastal and Offshore Engineering, Dalian University of Technology, Dalian 116023, People's Republic of China

² Institute of Fundamental Technological Research, Polish Academy of Sciences, 02-106 Warsaw, Poland

motion (Dolatabadi et al. 2020), apply Duhamel's integral (Law and Lin 2014), etc. If the system is linear and the noise is Gaussian, then the well-known Kalman filter can be used to handle the time-domain responses (Astroza et al. 2016). To improve numerical efficiency, the Fourier transform is used to change time-domain signals into frequency-domain signals. Li et al. (2012) proposed to reconstruct frequency-domain responses by transforming the measured responses into responses at other locations with the transmissibility matrix. Zhang and Aoki (2020) proposed a method for direct identification of structural parameters by using the frequency-domain responses, and these parameters were used for damage detection. Lee and Shin (2002a, b) derived a frequency-domain method of damage identification from the dynamic stiffness equation of motion. In the process of optimization, structural system matrices must be repeatedly reconstructed. To improve the efficiency of this process, fast structural reanalysis methods can be used, such as the virtual distortion method (VDM), see Kolakowski et al. (2008). Based on the VDM, Suwala and Jankowski (2012) proposed a method for off-line identification of modifications of structural mass. Zhang and Jankowski (2017) took advantage of the fast structural reanalysis by the VDM and used structural modes to identify damages. Lin et al. (2017) applied the VDM to damage detection in bridge engineering using its static and dynamic formulations. By the VDM, large quantities of structural dynamic data can be obtained and their sensitivity to the structural damage can be improved, which facilitates precise damage identification. The construction of structural responses relies on the stiffness, mass, and damping matrices (Adhikari and Woodhouse 2001), none of which are unnecessary. Structural damage is usually defined through stiffness, but to precisely identify location and degree of the damage with time-domain and frequency-domain methods, accurate mass, and damping data should be also known. However, damping phenomena in practical engineering are complex, and it is usually difficult to build an accurate damping matrix. Usually, the damping is approximated by using the Rayleigh damping model, which does not have a good performance when simulating the real damping (Adhikari 2006). Therefore, the error between practical and estimated damping can influence the precision of damage identification.

Structural modes are the most important dynamic characteristics of the structure. Modal analysis methods can be used to identify structural modes according to time- and frequency-domain responses. Structural frequencies and modal shapes depend only on structural mass and stiffness. Thus, the influence of damping estimation errors on damage identification can be circumvented. Mode-based damage identification methods typically build objective functions according to the residual between the experimental and theoretical modes. After that, the objective function is

optimized to identify the damage. Natural frequencies and modal shapes are frequently used to determine the position and degree of structural damage. Salawu (1997) proved that natural frequency changes can be used to locate structural damages. Chang and Kim (2016) conducted an experiment with a steel frame bridge with an artificial damage, and the results showed that the reduction in frequency represented the loss of the global stiffness of the structure. Khatir et al. (2019) utilized the Local Frequencies Change Ratio (LFCR) and normalized Modal Strain Energy Indicator (nMSEDI) as indicators to identify damages in beam. Teaching–Learning–Based Optimization Algorithm (TLBO) was employed with two-dimensional Isogeometric Analysis (IGA) to optimize nMSEDI. The damage in a laboratory steel beam can be determined using the proposed method. In the same year, Khatir and Abdel Wahab (2019) extended IGA to eXtended IsoGeometric Analysis (XIGA) method based on Proper Orthogonal Decomposition and radial basis functions. Combined with Jaya and Cuckoo optimization, single and multiple damages in plate structures could be identified accurately. In the next year, Khatir et al. (2020) utilized Jaya algorithm to train Artificial Neural Network (ANN) models, different crack length on plates can be identified by the trained ANN model. Not only the natural frequency can be used, but also the structural FRF is a good reference for damage identification. Lee and Shin (2002a, b) introduced an FRF-based damage identification method, which quantitatively showed the effects of omission of high vibration modes and suggested two simple but notable strategies to setup a well-posed damage identification problem: (1) use different excitation frequencies and different measurement points, and (2) reduce the domain of the problem. Kim et al. (2003) proved that damage identification could be carried out using only a limited amount of modal information, which however needs to be accurate. In the process of modal identification, responses are often affected by ambient noise and temperature-related effects. The influence of environmental temperature can be eliminated in damage identification using multi-modal analysis (Gillich et al. 2019). To eliminate the impact of noise pollution, Bayesian theory was introduced to damage identification process. The difference between the traditional methods and Bayesian damage identification is that Bayesian methods provide probability distributions instead of single deterministic numbers, which better reflects practical situations. Beck et al. (1998) proposed a Bayesian model updating method, which quantifies uncertainty of model parameters to be identified in terms of the entropy and uses it as a criterion for optimal sensor placement. Later, researchers were developing the approach continuously. Sedehi et al. (2019) proposed a hierarchical Bayesian method in time-domain to improve the reliability and robustness of traditional Bayesian methods. Hoskere et al. (2019) proposed a Bayesian damage recognition method for miter

gate crack damage. Yan et al. (2015) considered uncertainties due to modeling errors and measurement noise in the Bayesian framework and proposed a guided Bayesian inference approach for the detection of multiple flaws in structures. Due to the consideration of uncertainty, the robustness of damage identification to noise can be improved (Huang et al. 2018). Hou et al. (2018) proposed the additional virtual mass method based on the Bayesian theory and proved it by a frame structure experiment.

However, effectiveness of mode-based methods is adversely influenced by the practical limitations related to the number and placement of measurement points and modal insensitivity to local damage. Modification of physical parameters of the monitored structures was proved to be an effective way to avoid these problems. Nalittlela et al. (1993) were the first to propose the method of adding a physical mass or stiffness to a structure. Thereafter, the approach was developed further: Dems and Mroz (2010) used additional control parameters (e.g., mass, support, load, or temperature) in combination with modal, static, and thermodynamic analysis to identify damage. Dackermann et al. (2011) added practical masses to a two-story framed structure to simulate frequency changes due to structural damages. Furthermore, to improve the precision of damage identification, Lu et al. (2017) comprehensively analyzed the values, numbers, and positions of additional masses. Rajendran and Srinivasan (2015) investigated additional mass methods and predicted that the inclusion of rotational degrees of freedom (DOFs) should play a significant part in adding mass for damage identification. Based on an additional mass, Mousavi et al. (2020) proposed a new signal reconstruction method used for damage detection of beams. However, in practice, it is usually difficult to add a real mass (or other parameters) to the structure. Such a mass must be large enough to influence the structural dynamics, but it can be then difficult to handle and attach, and it might even contribute to the damage by itself. Adding virtual physical parameters to the structure is more efficient in practical engineering. Zhang et al. (2020) derived general equations for virtual modifications, including virtual mass, stiffness, and damping. Zhang et al. (2018, 2019) proposed to use a virtual control system to improve the accuracy of substructure identification. Tang et al. (2006) investigated the relationship between the virtual flexibility matrix and local stiffness changes by adding virtual forces to the structure. Hou et al. (2013) proposed the additional virtual mass method for damage identification, which effectively avoided the problem of adding real masses to the structure. The method was subsequently applied to bridges, truss structures, and frame structures. There are two steps for the additional mass method: (1) the measured experimental time-domain excitation and response are utilized to construct the structural response as if the mass was physically added to the structure; (2) modal

characteristics of the new structure with the (virtually) added mass are identified using the obtained response, and used as a reference for damage identification. This method combines the advantages of time-domain methods and mode-based methods. Firstly, the response of the structure after the mass is added can have an increased sensitivity to the damage, which retains the advantages of time-domain methods. Secondly, by using structural modes the influence of damping and noise on damage identification is decreased. Typically, the additional virtual mass method determines the additional mass at first and then calculates the corresponding natural frequency of the modified structure. However, when the excitation frequency band is narrow, such an approach cannot be used. The mass estimation method, proposed by Hou et al. (2020), first determines the desired structural natural frequency and then calculates the corresponding additional mass. The mass is virtually added to the structure, and its natural frequency is verified and used as a reference for monitoring and damage identification.

However, objective functions based on the residual of natural frequencies require the frequencies to be repeatedly computed: each iteration and each additional virtual mass require a new eigen decomposition to be performed. The computational efficiency of such a process is relatively low.

In this paper, a novel objective function is proposed that directly involves the estimated masses instead of the natural frequencies to increase the computational efficiency. Additionally, the entire method is formulated in the Bayesian framework, which allows multiple experimental data to be effectively used and decreases the influence of ambient noise and measurement errors.

The remainder of this paper is organized as follows: Sect. 2 introduces the principles of the additional mass method. Section 3 explains the damage identification process based on the estimated additional virtual masses. Section 4 proposes a probabilistic formulation in the Bayesian framework. Section 5 verifies the proposed methods using three numerical examples of varying complexities. Finally, in Sect. 6, the proposed method is experimentally validated with a laboratory plane frame. The paper is concluded in Sect. 7.

2 Additional virtual masses

The additional virtual mass method is straightforwardly applicable because it requires only the excitation and the acceleration response of one certain DOF of the structure. Then, the dynamic response of the new structure can be numerically constructed, as if any mass was physically added to that DOF. If $f(\omega)$ is the Fast Fourier Transform (FFT) of the excitation and $a(\omega)$ is the FFT of the acceleration response in the same DOF, then the FRF is

$h(\omega) = a(\omega)/f(\omega)$. As derived in Hou et al. (2013), the FRF $h_V(\omega, m)$ of the same structure with an additional mass m added in the same DOF can be expressed as in Eq. (1). This formula can be employed to add any additional virtual mass m to a real structure. The FRF of the new structure with the added mass provides additional information for damage identification.

$$h_V(\omega, m) = \frac{a(\omega)}{f(\omega) + ma(\omega)} = \frac{h(\omega)}{1 + mh(\omega)} \quad (1)$$

A typical relationship between structural natural frequency and the value of the additional mass is shown in Fig. 1. Natural frequency decreases with the increase of the additional mass. The curve in Fig. 1 involves two variables: natural frequency and additional mass. Depending on which of them is known in advance, there are two ways to analyze the structure.

- (1) Determining the natural frequency according to the additional mass. Given the virtual mass m_V , the peak of $h_V(\omega, m_V)$ in the frequency domain is used to determine the natural frequency ω_V , and then ω_V is used for damage identification. A typical example can be found in the literature (Hou et al. 2018). This method requires that the additional mass m_V keeps the natural frequency within an appropriate excitation frequency band. If the band is $[\omega_a, \omega_b]$ as shown in Fig. 1, then ω_V happens to be outside and there is a need to readjust the additional mass value to m^* so that the corresponding natural frequency ω^* is within $[\omega_a, \omega_b]$. The adjustment process may need multiple trial calculations, which is inconvenient and time-consuming.

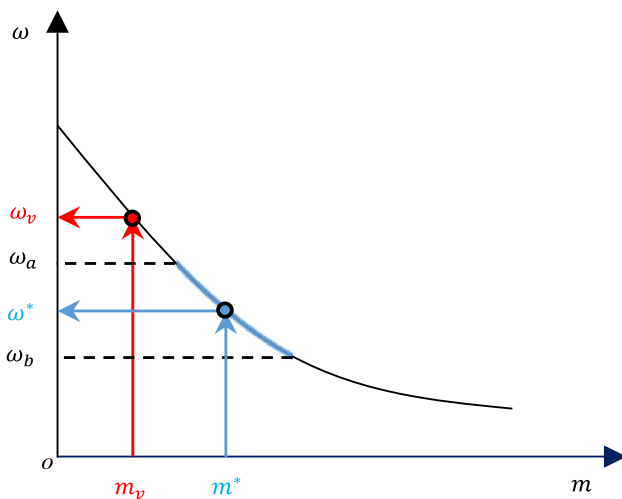


Fig. 1 Relationship between additional mass and natural frequency

- (2) Determining the additional mass according to the target frequency. To solve the problem of a narrow-band excitation, the expected natural frequency (named the target frequency) is determined first, and then the additional mass is estimated accordingly. Within the excitation frequency band $[\omega_a, \omega_b]$, given that the structural target frequency is ω^* , the corresponding additional mass can be obtained from the curve in Fig. 1 as m^* . Reference (Hou et al. 2020) proposed a direct and an improved additional mass estimation method using the geometric shape of $1/h(\omega)$ in the vicinity of ω^* , as shown in Fig. 2. The value $m^\#$ is obtained when the direct estimation method is used, see Eq. (2); the calculation is based on a single point of FRF, which is convenient, but the precision of mass estimation can be easily influenced. Therefore, the FRF data near ω^* are fitted to utilize the slope of the curve $1/h(\omega)$ and improve the precision of mass estimation. The improved estimated mass m^* can be calculated by Eq. (3),

$$m^\# = -\text{Re}(1/h(\omega^*)) \quad (2)$$

$$m^* = -\text{Re}(1/h(\omega^*)) - \text{Imag}(1/h(\omega^*))y'(\omega^*), \quad (3)$$

where Re represents the real part, Imag represents the imaginary part, and $y'(\omega^*)$ is the derivative of the (approximated) curve at the point A^* in Fig. 2.

To sum up, the method of estimating the virtual mass using the target frequency is not limited by the excitation bandwidth, and it is easily applicable in practical engineering. This paper develops on this basis. To improve the optimization efficiency and avoid the repeated calculation of the Eigen decomposition, a new objective function is established

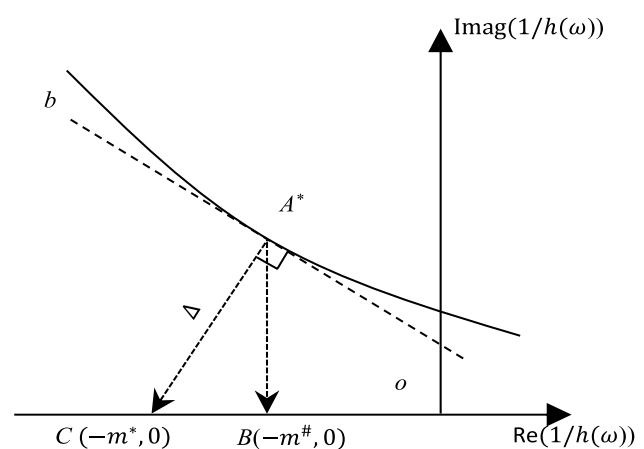


Fig. 2 Geometric interpretation of the direct and improved estimation methods

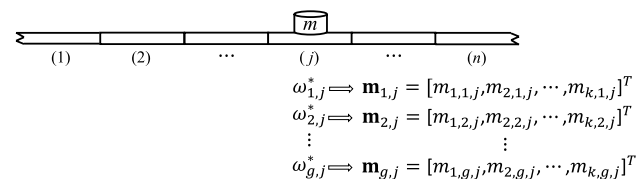
for damage identification based on the residual of the estimated additional mass. Furthermore, the proposed method is formulated in the Bayesian framework to improve the accuracy and reliability of damage identification.

3 Damage identification based on estimated additional virtual masses

3.1 Objective function based on additional virtual mass

As illustrated in Fig. 3, the structure to be identified is divided into n substructures. The coefficient μ_j denotes the damage factor of the j th substructure. It is defined as the ratio of the stiffness before and after the damage. Let $\boldsymbol{\mu} = [\mu_1, \mu_2, \dots, \mu_n]$. The stiffness matrix $\mathbf{K}(\boldsymbol{\mu})$ of the damaged structure can be calculated as $\mathbf{K}(\boldsymbol{\mu}) = \sum_j \mu_j \mathbf{K}_j$, where \mathbf{K}_j is the stiffness matrix of the j th substructure expressed in the global coordinate system.

After the virtual mass is added to the structure, the value of natural frequency is reduced. Adding masses in different positions of the structure has different influences on the structure. Therefore, the mass is added consecutively to different substructures. Assume that there are n substructures and g target frequencies at each position. For each target frequency, k dynamic experimental tests are performed. So there are $n \times g \times k$ sets of experimental data in total and each set is used to estimate a virtual mass value. Denote the i th target frequency of the j th substructure as $\omega_{i,j}^*$. In the p th experiment at the j th position using the i th target frequency, the additional mass is calculated by Eq. (3) as $m_{p,i,j}$. When $m_{p,i,j}$ is added to the FE model of the j th substructure, the corresponding i th frequency can be calculated as $\omega(\boldsymbol{\mu}, m_{p,i,j})$, where $\boldsymbol{\mu}$ is the damage factor. Reference Hou et al. (2020) uses the residual between the frequency $\omega(\boldsymbol{\mu}, m_{p,i,j})$ and the target frequency $\omega_{i,j}^*$ to establish the objective function Δ_ω , see Eq. (4). To identify the damage, the value of Δ_ω is minimized with respect to $\boldsymbol{\mu}$.

$$\Delta_\omega(\boldsymbol{\mu}) = \sum_{p,i,j} \left(\frac{\omega(\boldsymbol{\mu}, m_{p,i,j}) - \omega_{i,j}^*}{\omega_{i,j}^*} \right)^2$$


$$\begin{aligned} \omega_{1,j}^* &\Rightarrow \mathbf{m}_{1,j} = [m_{1,1,j}, m_{2,1,j}, \dots, m_{k,1,j}]^T \\ \omega_{2,j}^* &\Rightarrow \mathbf{m}_{2,j} = [m_{1,2,j}, m_{2,2,j}, \dots, m_{k,2,j}]^T \\ &\vdots \\ \omega_{g,j}^* &\Rightarrow \mathbf{m}_{g,j} = [m_{1,g,j}, m_{2,g,j}, \dots, m_{k,g,j}]^T \end{aligned}$$

Fig. 3 Calculation of additional masses using target frequencies

$$\Delta_\omega(\boldsymbol{\mu}) = \sum_{p,i,j} \left(\frac{\omega(\boldsymbol{\mu}, m_{p,i,j}) - \omega_{i,j}^*}{\omega_{i,j}^*} \right)^2 \quad (4)$$

However, the objective function based on the above frequency residual has some drawbacks:

- (1) Each additional mass $m_{p,i,j}$ estimated in the experiment must be added to the FE model to calculate the natural frequency. The calculation of Eq. (4) needs a large number of $n \times g \times k$ modifications of the structure and modal decompositions. It is computationally expensive.
- (2) Repetitively at each optimization step, this method uses the updated structural mass and stiffness matrices for all the above eigen decompositions anew. It additionally increases the computational cost of optimization and damage identification.

To improve the efficiency of optimization and to avoid the repeated eigen decomposition, a new objective function based on the virtual mass residual is established and proposed here:

$$\Delta_m(\boldsymbol{\mu}) = \sum_{p,i,j} \left(\frac{m(\boldsymbol{\mu}, \omega_{i,j}^*) - m_{p,i,j}}{m_{p,i,j}} \right)^2, \quad (5)$$

where $m(\boldsymbol{\mu}, \omega_{i,j}^*)$ is the additional virtual mass corresponding to the i th target frequency $\omega_{i,j}^*$ that needs to be added to the j th substructure of the FE model when the damage factor is $\boldsymbol{\mu}$. The objective function Eq. (5) does not need at all to calculate the eigenvalues of the structural system matrices. The optimization efficiency is thus much higher. In a single calculation of the objective function, only $n \times g$ additional virtual masses need to be computed. As discussed in the following sections, they can be quickly obtained in a direct way by using the FRF of the theoretical FE model.

3.2 Calculation of the additional virtual mass and its sensitivity analysis

To accurately calculate the additional virtual mass $m(\boldsymbol{\mu}, \omega_{i,j}^*)$ using the theoretical FE model under a certain damage factor $\boldsymbol{\mu}$, the following three issues need to be considered:

- (1) It is known from Eqs. (2) and (3) that the additional virtual mass can be estimated by using the FRF. Therefore, the FRF of the structure under a certain damage factor is the key to estimate the virtual mass. This section discusses two methods of calculating the structural FRF based on structural system matrices and the VDM.

- (2) The natural frequency of the structure is related to the stiffness and mass matrices of the structure, but not to the damping. Therefore, for the theoretical FE model, the damping can be neglected to eliminate its influence on the virtual mass estimation and to ensure that the required additional virtual mass is accurately calculated.
- (3) The derivation of the mass sensitivity to the damage factor helps to improve the efficiency of optimization and damage identification.

3.2.1 Calculation of virtual masses based on structural matrices

(1) Virtual mass estimation: If $\boldsymbol{\mu}$ denotes the damage factors of the FE model and the structural damping is neglected, the acceleration frequency response matrix can be calculated using the structural mass matrix \mathbf{M} and the stiffness matrix $\mathbf{K}(\boldsymbol{\mu})$. Denote the DOF number at which the additional mass is added by n_T . Let $\boldsymbol{\tau} = [0, 0, \dots, 1, \dots, 0, 0]^T$, which is 1 only in the n_T -th entry, and the remaining entries are 0. When the target frequency is ω , the acceleration frequency-domain response at ω is $h(\boldsymbol{\mu}, \omega)$ as in Eq. (6).

$$h(\boldsymbol{\mu}, \omega) = -\boldsymbol{\tau}^T \omega^2 (-\omega^2 \mathbf{M} + \mathbf{K}(\boldsymbol{\mu}))^{-1} \boldsymbol{\tau} \quad (6)$$

Since damping is ignored, the FRF of the structure has no imaginary part, that is, $y'(\omega^*)$ in Eq. (3) is 0, and Eq. (2) and Eq. (3) are the same. Therefore, for the target frequency ω , the frequency-domain response $h(\boldsymbol{\mu}, \omega)$ can be used to quickly estimate the additional virtual mass $m(\boldsymbol{\mu}, \omega)$ according to Eq. (2):

$$m(\boldsymbol{\mu}, \omega) = -\frac{1}{h(\boldsymbol{\mu}, \omega)} = -\frac{1}{\boldsymbol{\tau}^T H(\boldsymbol{\mu}, \omega) \boldsymbol{\tau}}. \quad (7)$$

The virtual mass estimated using Eq. (7) is accurate, because (a) $h(\boldsymbol{\mu}, \omega)$ is calculated by the mass matrix \mathbf{M} and the stiffness matrix $\mathbf{K}(\boldsymbol{\mu})$, so that it is the exact response of the FE model without the influence of noise or measurement errors; (b) since the damping is 0, the structural natural frequency is consistent with the peak position of the frequency-domain response.

In summary, for the theoretical FE model, the value of the additional virtual mass can be directly calculated using the mass and stiffness matrices of the structure, without modal decomposition, for any target frequency ω^* . If the number of structural DOFs is N , matrix inversion and eigen decomposition are both of the same time complexity $O(N^3)$, but for large matrices ($> 1000 \times 1000$), the operation of inversion is typically faster than the eigen decomposition by a factor of about three.

(2) Sensitivity of virtual mass to damage factor: if the sensitivity of the virtual mass Eq. (7) to the damage factor can be obtained, the optimization efficiency will be greatly improved by employing gradient-based optimization algorithms. The derivative of the estimated additional virtual mass $m(\boldsymbol{\mu}, \omega)$ with respect to the damage factor μ_l is called mass sensitivity, and it can be expressed as is shown in Eq. (8).

$$\frac{\partial m(\boldsymbol{\mu}, \omega)}{\partial \mu_l} = \frac{1}{\omega^2} \frac{\boldsymbol{\tau}^T H(\boldsymbol{\mu}, \omega) \mathbf{K}_l H(\boldsymbol{\mu}, \omega) \boldsymbol{\tau}}{h^2(\boldsymbol{\mu}, \omega)}, \quad (8)$$

where \mathbf{K}_l is the stiffness matrix of the l th substructure expressed in the global coordinate system, and μ_l is the damage factor of the l th substructure.

3.2.2 Calculation of virtual masses based on the VDM

(1) Quick construction of the FRF based on the VDM: The key step of using the FE model to estimate the virtual mass is to obtain the acceleration FRF $h(\omega, \boldsymbol{\mu})$ of the structure under a given damage factor $\boldsymbol{\mu}$. When the number of structural DOFs is relatively large, the inversion of the dynamic stiffness matrix in Eq. (6) is still relatively time-consuming. Therefore, the VDM, which is a fast structural reanalysis method, can be used to quickly construct the FRF. This section presents the basic formulas, while their derivation and interpretation can be found in references Kolakowski et al. (2008), Suwala and Jankowski (2012), Zhang and Jankowski (2017), or Lin et al. (2017). If $h^L(\omega)$ is the acceleration FRF of the undamaged structure, then according to the VDM, $h(\boldsymbol{\mu}, \omega)$ and $h^L(\omega)$ are related to each other as

$$h(\boldsymbol{\mu}, \omega) = h^L(\omega) + \sum_{\alpha} \sum_l D_{\alpha l}^{\gamma}(\omega) \gamma_{\alpha l}^0(\omega). \quad (9)$$

According to Eq. (9), the damage is equivalently modeled with the virtual distortions that act in the undamaged structure. The symbol $\gamma_{\alpha l}^0(\omega)$ denotes the amplitude of the α th virtual distortion of the l th substructure (excitation in the coordinate of the respective virtual distortion $\boldsymbol{\vartheta}_{\alpha l}$), and $D_{\alpha l}^{\gamma}(\omega)$ is the corresponding frequency-domain response of the undamaged structure to a unit harmonic virtual distortion. The virtual distortions $\boldsymbol{\vartheta}_{\alpha l}$ are defined as eigenvectors that correspond to the positive eigenvalues of the stiffness matrix \mathbf{K}_l of the l th substructure, $\mathbf{K}_l = \sum_{\alpha} \lambda_{\alpha l} \boldsymbol{\vartheta}_{\alpha l} \boldsymbol{\vartheta}_{\alpha l}^T$. The damage-equivalent excitations $\gamma_{\alpha l}^0(\tau)$ can be shown to depend on the damage factor $\boldsymbol{\mu}$ and the FRF of the undamaged structure as follows:

$$(1 - \mu_l) \gamma_{\alpha l}^L(\omega) = \gamma_{\alpha l}^0(\omega) - (1 - \mu_l) \sum_{\eta} \sum_{\xi} D_{\alpha \eta \xi}(\omega) \gamma_{\eta \xi}^0(\omega), \quad (10)$$

where $\gamma_{\alpha l}^L(\omega)$ is the FRF of the undamaged structure in the virtual distortion coordinate $\boldsymbol{\vartheta}_{\alpha l}$, $D_{\alpha \eta \xi}(\omega)$ is the corresponding frequency-domain response of the undamaged structure

to a unit harmonic virtual distortion $\mathbf{\Theta}_{\eta_i^*}$, and μ_l denotes the damage factor of the l th substructure. Stated in the matrix form, Eq. (9) and Eq. (10) yield together

$$h(\boldsymbol{\mu}, \omega) = h^L(\omega) + \mathbf{D}^T (\mathbf{I} - (\mathbf{I} - [\boldsymbol{\mu}]) \mathbf{D})^{-1} (\mathbf{I} - [\boldsymbol{\mu}]) \boldsymbol{\gamma}^L(\omega), \quad (11)$$

where $[\boldsymbol{\mu}]$ is the diagonal matrix $\text{diag}(\boldsymbol{\mu})$, while \mathbf{D}^T and \mathbf{D} denote matrices with appropriately arranged coefficients $D_{al}^T(\omega)$ and $D_{al\eta_i^*}(\omega)$.

After $h(\boldsymbol{\mu}, \omega)$ is obtained using Eq. (11), the additional virtual mass $m(\boldsymbol{\mu}, \omega)$ for the target frequency ω can be calculated by Eq. (7). The computational cost of the VDM-based method described above is $O(N_\lambda^3)$, where N_λ is the total number of virtual distortions of all considered substructures. It should be noted that in typical applications N_λ is often just a fraction of the total number of all structural DOFs, $N_\lambda \ll N$ (Zhang and Jankowski 2017).

(2) Sensitivity analysis of virtual mass based on the VDM: Differentiating Eq. (11) with respect to the damage factor yields

$$\frac{\partial h(\boldsymbol{\mu}, \omega)}{\partial \mu_l} = \mathbf{D}^T (\mathbf{I} - (\mathbf{I} - [\boldsymbol{\mu}]) \mathbf{D})^{-1} (\mathbf{I}_l \mathbf{D}) (\mathbf{I} - (\mathbf{I} - [\boldsymbol{\mu}]) \mathbf{D})^{-1} (\mathbf{I} - [\boldsymbol{\mu}]) \boldsymbol{\gamma}^L(\omega) - \mathbf{D}^T (\mathbf{I} - (\mathbf{I} - [\boldsymbol{\mu}]) \mathbf{D})^{-1} \mathbf{I}_l \boldsymbol{\gamma}^L(\omega), \quad (12)$$

where \mathbf{I}_l are partitioned unit matrices that correspond to the arrangement of the damage factors, $[\boldsymbol{\mu}] = \sum_l \mu_l \mathbf{I}_l$. By using the shorthand notation $U_l = \frac{\partial h(\boldsymbol{\mu}, \omega)}{\partial \mu_l}$, $\mathbf{G} = \mathbf{I} - [\boldsymbol{\mu}]$ and $\mathbf{F} = (\mathbf{I} - (\mathbf{I} - [\boldsymbol{\mu}]) \mathbf{D})^{-1}$, Eq. (12) can be rewritten in a simpler form as Eq. (13),

$$U_l = \mathbf{D}^T \mathbf{F} \mathbf{I}_l \mathbf{D} \mathbf{F} \mathbf{G} \boldsymbol{\gamma}^L(\omega) - \mathbf{D}^T \mathbf{F} \mathbf{I}_l \boldsymbol{\gamma}^L(\omega). \quad (13)$$

The mass sensitivity is obtained as shown in Eq. (14), where $h(\boldsymbol{\mu}, \omega)$ is the same as in Eq. (11).

$$\frac{\partial m(\boldsymbol{\mu}, \omega)}{\partial \mu_l} = h^{-2}(\boldsymbol{\mu}, \omega) U_l \quad (14)$$

To compare the methods based on structural system matrices and the VDM, it should be noted that both methods can be used to determine the additional virtual mass and its exact sensitivity. Selection of the specific method depends on the specific structure:

- When the number of structural DOFs N is close to the total number of virtual distortions N_λ , the first method based on structural system matrices is recommended due to its simplicity.
- When the number of structural DOFs N is much larger than the total number of virtual distortions N_λ , the second method based on the VDM is recommended because it is numerically more efficient in optimization.

3.3 Damage identification based on virtual mass sensitivity

The previous sections demonstrated that the virtual mass can be calculated by Eq. (7), while its derivative with respect to the damage factors can be quickly found by Eq. (8) or Eq. (14). This allows any gradient-based optimization method to be employed for minimization of the objective function Eq. (5) and damage identification. The Newton method is used in this work. To this end, the virtual mass $m(\boldsymbol{\mu}, \omega_{i,j}^*)$ is linearized around $\boldsymbol{\mu}_0$, and in line with Eq. (5), compared to the experiment-based mass $m_{p,i,j}$:

$$m(\boldsymbol{\mu}, \omega_{i,j}^*) \approx m(\boldsymbol{\mu}_0, \omega_{i,j}^*) + \frac{\partial m(\boldsymbol{\mu}_0, \omega_{i,j}^*)}{\partial \boldsymbol{\mu}} (\boldsymbol{\mu} - \boldsymbol{\mu}_0) = m_{p,i,j}. \quad (15)$$

Equation (15) is then rearranged and normalized by dividing its sides by $m_{p,i,j}$. Finally, all indices p (experimental tests), i (target frequencies), and j (substructures) are collected. The resulting linear system is overdetermined, as it has $n \times g \times k$ equations, but only n unknown damage factors. Note that its solution in the least squares sense corresponds to the minimum of the objective function Eq. (5). This allows the iteration of the Newton method to be formulated as follows:

$$\boldsymbol{\mu}_{i+1} = \boldsymbol{\mu}_i + (\mathbf{E}^{-1} \mathbf{Q}(\boldsymbol{\mu}_i, \boldsymbol{\omega}^*))^\# \mathbf{E}^{-1} (\mathbf{m}_m - \mathbf{m}(\boldsymbol{\mu}_i, \boldsymbol{\omega}^*)), \quad (16)$$

where the subscript $\#$ denotes the matrix pseudoinverse (Moore–Penrose inverse), the column vector \mathbf{m}_m collects all the experiment-based masses $m_{p,i,j}$, the matrix $\mathbf{E} = \text{diag}(\mathbf{m}_m)$ is the respective normalization matrix, and the Jacobian matrix $\mathbf{Q}(\boldsymbol{\mu}_i, \boldsymbol{\omega}^*)$ consists of the appropriately arranged sensitivities $\partial m(\boldsymbol{\mu}, \omega_{i,j}^*) / \partial \mu_l$ collected for all i, j, l and repeated for all k experimental tests. In the iterative optimization process, the initial damage factors correspond to the undamaged structure $\boldsymbol{\mu}_0 = [1, 1, \dots, 1]^T$.

An iterative optimization formula similar to Eq. (16) can be derived also for the frequency-based objective function Eq. (4) as follows:

$$\boldsymbol{\mu}_{i+1} = \boldsymbol{\mu}_i + \left((\mathbf{E}')^{-1} \mathbf{R}(\boldsymbol{\mu}_i, \mathbf{m}_m) \right)^\# (\mathbf{E}')^{-1} (\boldsymbol{\omega}^* - \boldsymbol{\omega}(\boldsymbol{\mu}_i, \mathbf{m}_m)), \quad (17)$$

where $\boldsymbol{\omega}(\boldsymbol{\mu}, \mathbf{m}_m)$ is the column vector of natural frequencies obtained by adding to the FE model all the experiment-based additional virtual masses $m_{p,i,j}$, the vector $\boldsymbol{\omega}^*$ collects and appropriately arranges all the target frequencies $\omega_{i,j}^*$, $\mathbf{R}(\boldsymbol{\mu}, \mathbf{m}_m)$ is the appropriately arranged sensitivity matrix of natural frequencies with respect to the damage factors (Hou

et al. 2013), and $\mathbf{E}' = \text{diag}(\boldsymbol{\omega}^*)$ is the corresponding diagonal weighting matrix.

4 Damage identification method based on Bayesian theory

Assume that the damage factors are independent and that their prior is normal. Their prior joint probability density function is thus as follows:

$$P(\boldsymbol{\mu}) = c_1 \cdot \exp\left[-\frac{1}{2}(\boldsymbol{\mu} - \bar{\boldsymbol{\mu}}_0)^T \mathbf{S}^{-1}(\boldsymbol{\mu} - \bar{\boldsymbol{\mu}}_0)\right], \quad (18)$$

where c_1 is a normalization constant, $\bar{\boldsymbol{\mu}}_0$ is the initial value of the damage factor, generally $\bar{\boldsymbol{\mu}}_0 = [1, 1, \dots, 1]^T$, and \mathbf{S} denotes the diagonal matrix with the variances of the damage factor at the diagonal.

This section uses the additional masses $m_{p,i,j}$ estimated for the structural target frequencies as an evidence \mathbf{D} for damage identification in Bayesian framework. Under the usual assumption of measurement data independence, the posterior probability distribution of the damage factors can be written in the following form, where the meaning of the subscripts is the same as in Sect. 3.1:

$$P(\boldsymbol{\mu}|\mathbf{D}) = c_1 P(\boldsymbol{\mu}) \cdot P(\mathbf{D}|\boldsymbol{\mu}) = c_1 P(\boldsymbol{\mu}) \prod_{j=1}^n \prod_{i=1}^g \prod_{p=1}^k P(m_{p,i,j}|\boldsymbol{\mu}), \quad (19)$$

where the probability density function of the additional mass estimated for a structural target frequency is as shown in Eq. (20),

$$P(m_{p,i,j}|\boldsymbol{\mu}) = c_2 \cdot \exp\left[-\frac{1}{2}\left(\frac{m(\boldsymbol{\mu}, \omega_{i,j}^*) - m_{p,i,j}}{\tilde{\sigma}_{i,j}}\right)^2\right], \quad (20)$$

where $m(\boldsymbol{\mu}, \omega_{i,j}^*)$ can be obtained by Eq. (7), $\tilde{\sigma}_{i,j}$ is the standard deviation of the k virtual masses $\mathbf{m}_{i,j} = [m_{1,i,j}, m_{2,i,j}, \dots, m_{k,i,j}]$ estimated for the i th target frequency at the j th substructure, see Fig. 3. The posterior probability of the damage factors is thus as shown in Eq. (21) and Eq. (22):

$$P(\boldsymbol{\mu}|\mathbf{D}) = c \cdot \exp[J(\boldsymbol{\mu})] \quad (21)$$

$$J(\boldsymbol{\mu}) = -\frac{1}{2}(\boldsymbol{\mu} - \bar{\boldsymbol{\mu}}_0)^T \mathbf{S}^{-1}(\boldsymbol{\mu} - \bar{\boldsymbol{\mu}}_0) - \frac{1}{2}(\mathbf{m}(\boldsymbol{\mu}) - \mathbf{m}_m)^T \boldsymbol{\Gamma}^{-1}(\mathbf{m}(\boldsymbol{\mu}) - \mathbf{m}_m), \quad (22)$$

where c is a normalization constant, the vector \mathbf{m}_m collects all the masses $m_{p,i,j}$, while $\mathbf{m}(\boldsymbol{\mu})$ denotes the respectively

arranged vector of the corresponding FE-based values $m(\boldsymbol{\mu}, \omega_{i,j}^*)$, and $\boldsymbol{\Gamma}$ is the diagonal matrix of the respectively arranged variances $\tilde{\sigma}_{i,j}^2$.

The posterior probability described by Eq. (21) is approximated by a normal probability with the mean at the maximum of $J(\boldsymbol{\mu})$. To find the maximum, the gradient of $J(\boldsymbol{\mu})$ with respect to $\boldsymbol{\mu}$ is calculated. By comparing it to the vector of zeros, Eq. (23) is obtained:

$$\mathbf{S}^{-1}(\boldsymbol{\mu} - \bar{\boldsymbol{\mu}}_0) + \mathbf{Q}^T(\boldsymbol{\mu})\boldsymbol{\Gamma}^{-1}(\mathbf{m}(\boldsymbol{\mu}) - \mathbf{m}_m) = \{0\}, \quad (23)$$

where $\mathbf{Q}(\boldsymbol{\mu})$ is the appropriately rearranged mass sensitivity matrix $\partial \mathbf{m}(\boldsymbol{\mu})/\partial \boldsymbol{\mu}$, the same as in Eq. (16). By substituting the first-order Taylor formula for $\mathbf{m}(\boldsymbol{\mu})$ into Eq. (23), the following iterative formula for the damage factor can be obtained:

$$\boldsymbol{\mu}_{i+1} = \mathbf{B}(\boldsymbol{\mu}_i)\bar{\boldsymbol{\mu}}_0 + \mathbf{C}(\boldsymbol{\mu}_i)\mathbf{m}_m + \mathbf{d}(\boldsymbol{\mu}_i), \quad (24)$$

where

$$\begin{cases} \mathbf{B}(\boldsymbol{\mu}_i) = (\mathbf{S}^{-1} + \mathbf{Q}^T(\boldsymbol{\mu}_i)\boldsymbol{\Gamma}^{-1}\mathbf{Q}(\boldsymbol{\mu}_i))^{-1}\mathbf{S}^{-1} \\ \mathbf{C}(\boldsymbol{\mu}_i) = (\mathbf{S}^{-1} + \mathbf{Q}^T(\boldsymbol{\mu}_i)\boldsymbol{\Gamma}^{-1}\mathbf{Q}(\boldsymbol{\mu}_i))^{-1}\mathbf{Q}^T(\boldsymbol{\mu}_i)\boldsymbol{\Gamma}^{-1} \\ \mathbf{d}(\boldsymbol{\mu}_i) = (\mathbf{S}^{-1} + \mathbf{Q}^T(\boldsymbol{\mu}_i)\boldsymbol{\Gamma}^{-1}\mathbf{Q}(\boldsymbol{\mu}_i))^{-1}\mathbf{Q}^T(\boldsymbol{\mu}_i)\boldsymbol{\Gamma}^{-1}(\mathbf{Q}^T(\boldsymbol{\mu}_i)\boldsymbol{\mu}_i - \mathbf{m}(\boldsymbol{\mu}_i)) \end{cases} \quad (25)$$

Let the initial value of damage factor be $\boldsymbol{\mu}_0 = [1, 1, \dots, 1]^T$ and $\bar{\boldsymbol{\mu}}_0 = [1, 1, \dots, 1]^T$. Then, the posterior probability of the damage factors is approximated by the normal distribution with the result optimized by Eq. (24) as the mean value. The variance of damage factors can be calculated with Eq. (26):

$$\boldsymbol{\sigma}^2 = \text{diag}(\mathbf{S}^{-1} + \mathbf{Q}^T(\boldsymbol{\mu})\boldsymbol{\Gamma}^{-1}\mathbf{Q}(\boldsymbol{\mu}))^{-1}. \quad (26)$$

5 Numerical verification

This section verifies the proposed method using three numerical examples: a simply supported beam, a 3D truss structure, and a 3D model of a 3-story building.

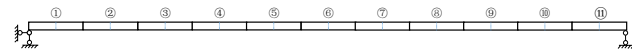
5.1 Simply supported beam

5.1.1 Numerical model

A FE model of a simply supported beam is used to perform the process of damage identification and to compare the assumed and identified values of damage factors. The parameters of the beam are listed in Table 1. The beam is divided into 11 substructures and each of them has 2 elements (see Fig. 4). Given the target frequency, the corresponding mass added to the middle of each substructure

Table 1 Parameters of the simply supported beam

Length	Young's modulus	Density	Poisson's ratio	Cross-section width	Cross-section height
2.1 m	210 GPa	7850 kg/m ³	0.3	80 mm	35 mm

**Fig. 4** Division of the beam into substructures

is found. Finally, the additional virtual mass estimation method based on Bayesian theory is used to perform damage identification.

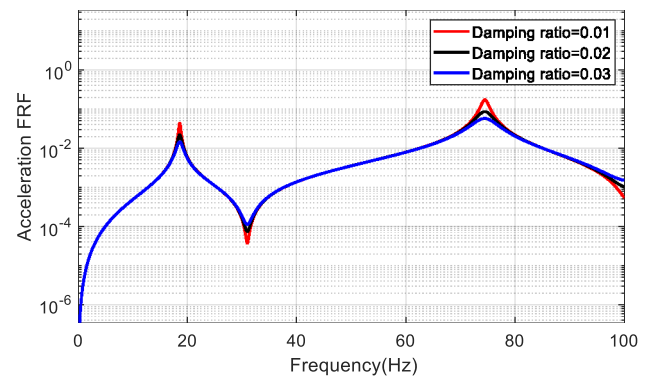
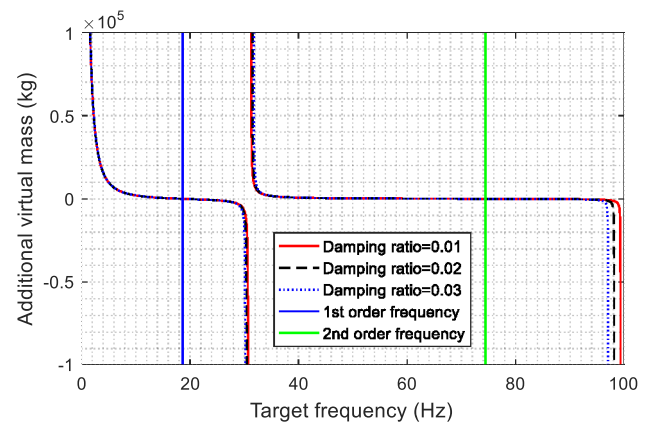
Based on the parameters listed in Table 1, the first four natural frequencies of the beam can be calculated as 18.6 Hz, 74.5 Hz, 167.5 Hz, and 297.8 Hz. By local structural sensitivity analysis, the first natural frequency is selected to be used for damage identification.

5.1.2 Construction and comparison of additional virtual masses

5.1.2.1 Verification of additional mass estimation using the FE model For the intact structure, assuming that the target frequency is 15 Hz for each substructure, the additional masses can be calculated by Eq. (7). For example, for the 2nd substructure, the calculated FRF is $h_2(\boldsymbol{\mu}, \omega) = -0.0154$, so the additional mass is calculated as $m_2 = 65.0379\text{kg}$. Indeed, if mass m_2 is added to the 2nd substructure of the FE model, the new natural frequency is calculated as 15 Hz, which confirms the validity of Eq. (7).

5.1.2.2 FRF construction for a damaged beam The damage factors $\boldsymbol{\mu} = [1, 1, 0.8, 1, 1, 0.5, 1, 1, 1, 0.5, 1]$ are assumed. The FRFs can be calculated by the method based on the structural mass and stiffness matrices \mathbf{M} and $\mathbf{K}(\boldsymbol{\mu})$, as well as by the VDM method. Take the 1st substructure as an example. Let the target frequency be 15 Hz. The FRF can be calculated as $h_1(\boldsymbol{\mu}, \omega) = -0.0036$. The additional mass is $m_1 = 276.1353\text{kg}$ and its sensitivity with respect to μ_1 is computed as 171.4047. Both methods yield exactly the same values, which confirms their validity and precision.

The beam has 63 DOFs. Through the Eigen decomposition of the substructure stiffness matrix \mathbf{K}_l , the number of virtual distortions (VDs) of each substructure is found to be 6, so that the beam has 66 VDs in total. For the proposed beam, the numbers of the DOFs and VDs are nearly the same, so that the method based on \mathbf{M} and $\mathbf{K}(\boldsymbol{\mu})$ is more efficient and therefore employed.

**Fig. 5** Acceleration FRF of the first substructure**Fig. 6** Additional mass estimated by the target frequency for substructure 1

5.1.3 Sensitivity of virtual masses

As discussed in Sect. 3.3, the mass sensitivity matrix \mathbf{Q} is an important factor required by the proposed damage identification method. Consider the first substructure of the intact beam, $\boldsymbol{\mu}_0 = [1, 1, 1, 1, 1, 1, 1, 1, 1, 1, 1]$. The Rayleigh damping model is considered, and the first two modal damping ratios are the same. The excitation is applied to the middle position of the substructure and the corresponding acceleration response is measured at the same point. Figure 5 shows the corresponding acceleration FRF $h(\boldsymbol{\mu}_0, \omega)$ computed for the damping ratios of 0.01, 0.02, and 0.03. Under different damping ratios, the FRFs of the structure are different. In case of a physical structure, the actual damping might be unknown or inaccurately identified. In such cases, the accuracy of damage identification can be affected if the structural FRF is directly used.

Figure 6 shows the corresponding additional masses, as computed by Eq. (3). It can be seen that the curves corresponding to the three considered damping ratios are nearly indistinguishable for the entire range of the target

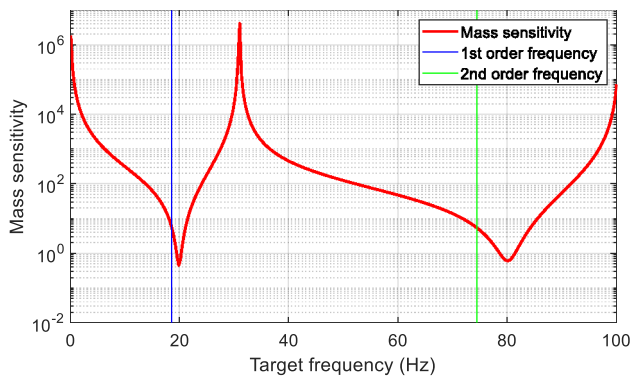


Fig. 7 Sensitivity of virtual mass with respect to the damage factor of substructure 1

frequencies except for two small ranges near the two antiresonance points (around 31 Hz and 98 Hz). It confirms that the proposed method is nearly not influenced by the damping, especially that it is recommended to select the target frequencies far from the antiresonance points in order to ensure a high signal-to-noise ratio.

The selection of the target frequency is tightly associated with mass sensitivity, FRF amplitude, and structural natural frequency. Figure 7 plots the sensitivity of the additional virtual mass with respect to the damage factor of the first substructure.

When the target frequency is not very close to the natural frequency, it can be seen from Figs. 5, 6, and 7 that the higher the FRF amplitude is, the smaller the corresponding additional mass and mass sensitivity are; in contrast, when the FRF amplitude is smaller, the additional mass and mass sensitivity are greater. Greater mass sensitivities are conducive to the accuracy of damage identification. Therefore, to improve mass sensitivity, the selected target frequency ought to be far away from the structural natural frequency.

However, when the target frequency is too far from the natural frequency, the amplitude of the FRF is small. Under the same level of measurement noise, the smaller the FRF amplitude is, the greater the influence of the noise is, and so is the error of mass estimation. Hence, in order to decrease the detrimental effects of noise contamination, the selected target frequency should not be too far from the structural natural frequency.

To further illustrate the selection of the target frequency, the mass sensitivities are computed for all substructures and shown in Fig. 8. When the target frequency is near the natural frequency of the beam, all sensitivities tend to be almost zero. When the target frequency is less than the natural frequency, all mass sensitivities increase with the decrease of the target frequency, and the relationship between them is consistent. But when the target frequency increases beyond the natural frequency, mass sensitivities first decrease and

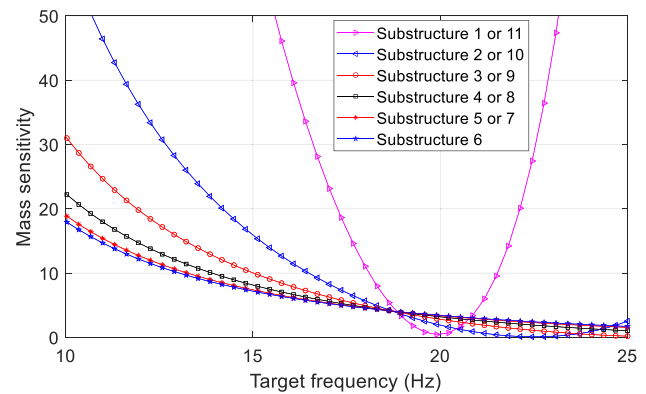


Fig. 8 Comparison of virtual masses sensitivity for all 11 substructures

then increase, and most of them remain relatively low. The relationship between them becomes less consistent. Furthermore, when the target frequency is larger than the structural natural frequency, the calculated additional mass is negative, see Fig. 6. Negative mass value means that the corresponding mass should be subtracted from the considered position of the structure. Such a negative mass is not physical, and it cannot induce high structural sensitivity, as shown in Fig. 8. It suggests that the target frequency should be smaller than the natural frequency.

Overall, the selection of the target frequency should equally consider the mass sensitivity, the signal-to-noise ratio, and the consistency of the relationship between the target frequency and mass sensitivity. Based on this criterion, the target frequency should be smaller than the natural frequency, and at a certain distance from it, but this distance should not be too large.

5.1.4 Structural dynamic tests and additional mass estimation

In this section, we use 3 damage scenarios to perform damage identification:

Scenario 1: $\mu = [1, 0.4, 1, 1, 0.5, 1, 1, 1, 0.8, 1, 1]$, mixed small and large damage;

Scenario 2: $\mu = [1, 1, 1, 1, 0.9, 1, 1, 1, 1, 1, 1]$, single small damage;

Scenario 3: $\mu = [1, 1, 1, 1, 0.2, 1, 1, 1, 1, 1, 1]$, single large damage.

Based on the analysis in Sect. 5.1.3, the target frequency is selected as 13 Hz. The same frequency is also selected for the excitation in order to obtain the frequency response data of the structure at the target frequency. The excitation time is $T_f = 1.19$ s. In the numerical simulation process, the sampling frequency is 10 kHz. The applied excitation is shown in Fig. 9 (a) and modeled as

$$f(t) = \frac{1}{2} \sin(2\pi\omega_f t) (1 - \cos(2\pi t/T_f)) \text{ for } t \in [0, T_f]. \quad (27)$$

Take the first substructure as an example. The excitation Eq. (27) is applied, and the computed response of the substructure is shown in Fig. 9b. To simulate the effects of the ambient noise, 5% white noise is added to the excitation and to the response at the same time. To analyze the relationship between the additional mass and the natural frequency, the excitation and the response should be analyzed in frequency domain. The FFT transforms of both signals are shown in Fig. 10.

The above process is repeated for all substructures in scenario 1. Thereafter, given the target frequency of 13 Hz, the additional masses can be obtained by Eq. (3). In order

to decrease the influence of noise, 10 tests are executed for each substructure, so there are a total 110 tests for the entire beam. The calculated masses are shown in Table 2. For example, for substructure 3 in test 5 in scenario 1, for the target frequency 13 Hz, the estimated mass is calculated by Eq. (3) as 30.9 kg.

5.1.5 Damage identification

The same FE model is used for damage identification, and the initial damage factors in the optimization process correspond to the intact structure $\mu_0 = [1, 1, 1, 1, 1, 1, 1, 1, 1, 1]$. When the frequency residual objective function Eq. (4) is used, the damage factors are optimized using Eq. (17) and denoted by μ_ω . Similarly, when the mass residual objective

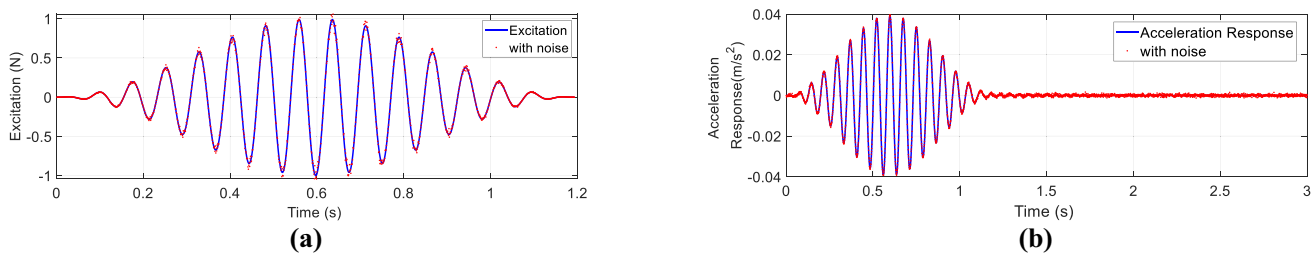


Fig. 9 Excitation and response: **a** Excitation, **b** Response

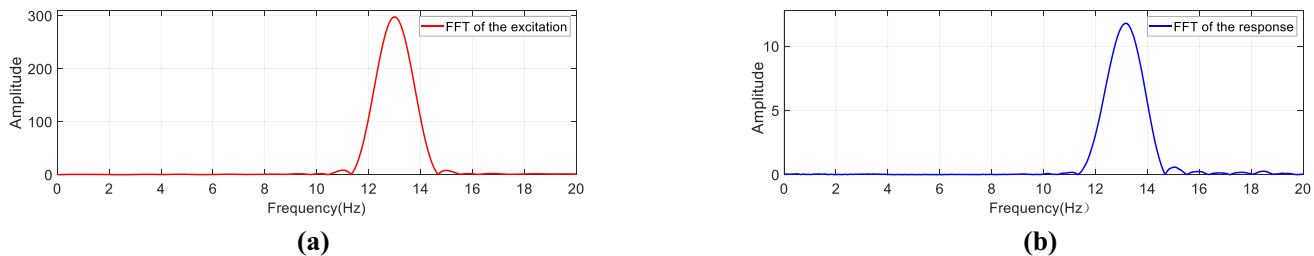


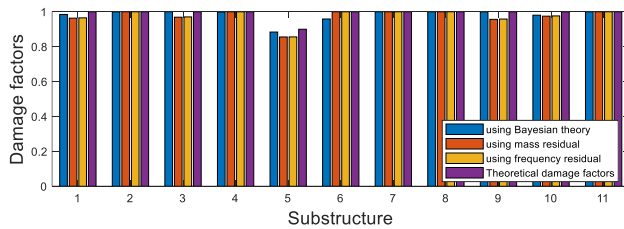
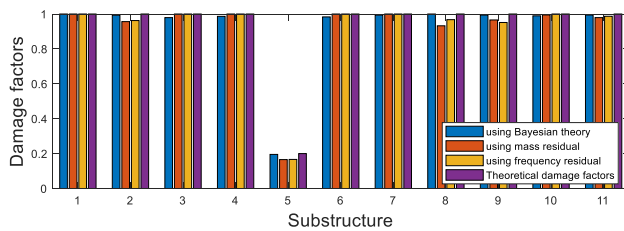
Fig. 10 FFT of the excitation and response: **a** Excitation, **b** Response

Table 2 Additional virtual masses (kg) estimated for each substructure for the target frequency of 13 Hz in scenario 1

Substructure	Test 1	Test 2	Test 3	Test 4	Test 5	Test 6	Test 7	Test 8	Test 9	Test 10
1	534.7	535.1	534.2	534.7	534.2	534.3	534.9	534.6	534.5	532.4
2	66.8	67.0	67.4	66.8	66.6	67.3	66.8	67.1	67	66.9
3	31.4	31.2	31.3	30.7	30.9	31.4	30.7	30.6	31	31.2
4	20.0	19.9	20.1	19.9	20.0	19.9	19.8	19.8	20.0	19.9
5	15.5	15.6	15.4	15.7	15.4	15.4	15.4	15.5	15.5	15.3
6	15.4	15.6	15.2	15.5	15.5	15.2	15.6	15.3	15.2	15.4
7	17.3	17.5	17.3	17.3	17.2	17.4	17.4	17.2	17.3	17.1
8	22.6	22.5	22.4	22.6	22.5	22.4	22.3	22.4	22.5	22.6
9	36.1	36.0	36.0	36.1	36.0	35.9	36	36.1	35.8	36.3
10	86.4	86.7	85.8	86.2	86.2	86.2	86.9	86.6	86.7	86.9
11	699.5	696.3	695.4	693.9	695.9	695.5	697.1	695.8	696.5	696.6

Table 3 Damage identification results in scenario 1

Substructure	1	2	3	4	5	6	7	8	9	10	11
Theoretical value	1.0000	0.4000	1.0000	1.0000	0.5000	1.0000	1.0000	1.0000	0.8000	1.0000	1.0000
μ_ω	0.9986	0.3932	0.9902	1.0000	0.4782	1.0000	0.9692	0.9537	0.8121	0.9858	0.9973
μ_m	0.9971	0.3927	0.9882	1.0000	0.4775	1.0000	0.9677	0.9524	0.8111	0.9844	0.9959
Mean value of μ	0.9762	0.4015	0.9584	0.9589	0.5326	0.9698	1.0000	0.9465	0.8254	0.9727	1.0000
Standard deviation of μ	0.0212	0.0055	0.0355	0.0321	0.013	0.0374	0.032	0.0259	0.0167	0.0201	0.0196

**Fig. 11** Damage identification for scenario 2**Fig. 12** Damage identification for scenario 3

function Eq. (5) is utilized, the damage factors are optimized by Eq. (16) and denoted by μ_m . It is worth noting that these three results are all deterministic. However, due to the presence of noise, the damage factors are nondeterministic, and the proposed Bayesian approach is used to calculate the damage factors. The acceleration FRF is computed by Eq. (6) and the additional mass is calculated by Eq. (7). Finally, the mean values of the damage factors are obtained by Eq. (24) and their covariance matrix is calculated by Eq. (26). For scenario 1: mixed small and large damage, all damage identification results are shown in Table 3.

For scenario 2: small damage, set the target frequency as 13 Hz, too. Using the estimated masses, damage factors can be identified as in Fig. 11. The standard deviation of the components of μ is [0.0342, 0.0335, 0.0383, 0.0322, 0.0141, 0.0440, 0.0427, 0.0406, 0.0388, 0.0358, 0.0392].

Furthermore, for scenario 3: large damage, the same process is performed, and the results are shown in Fig. 12. The corresponding standard deviation of the components of μ is [0.0368, 0.0283, 0.0333, 0.0366, 0.0111, 0.0365, 0.0312, 0.0389, 0.0371, 0.0308, 0.0238]. It can be seen that

Table 4 Number of iterations and the total computation time in scenario 1

	μ_ω	μ_m	Mean value of μ
Number of iterations	5	5	4
Time of iteration	1.1368 s	0.2183 s	0.1805s

the proposed method can be successfully applied to a single small damage and a single large damage as well.

Table 4 lists the number of iterations and the average computation time of each iteration for all four identification methods in scenario 1 used as an example. All methods yield their final results in no more than 5 iterations. The Bayesian identification method based on the estimated additional masses is the most efficient.

The relative error of the damage factor μ_2 (2nd substructure) after every iteration is listed as an example in Table 5. Both deterministic methods, based on the frequency and mass residuals, converge at the 5th iteration. However, the efficiency of the frequency-based method Eq. (4) is poor: it uses more time in each iteration because of the need for a repeated calculation of the eigenvalues. The method based on the mass residual Eq. (5) is much more time efficient. The mean values of the damage factor, as estimated with the proposed Bayesian approach, are relatively close to the assumed actual values. The standard deviations of μ are relatively small. The errors between the estimated mean values of μ and the actual values are within 5%, and the mean deviation equals 1.1 σ . Such values are permitted in practical engineering.

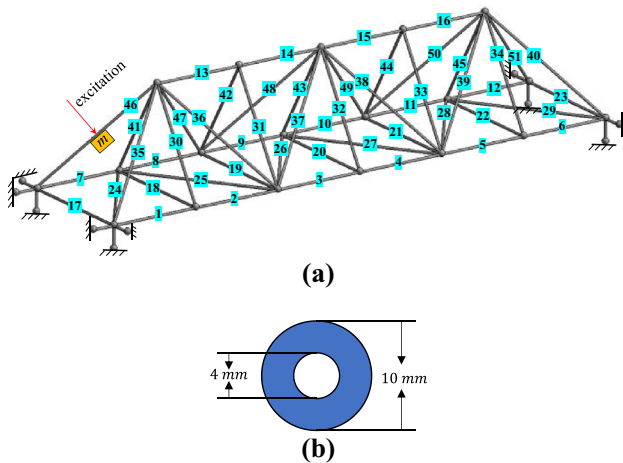
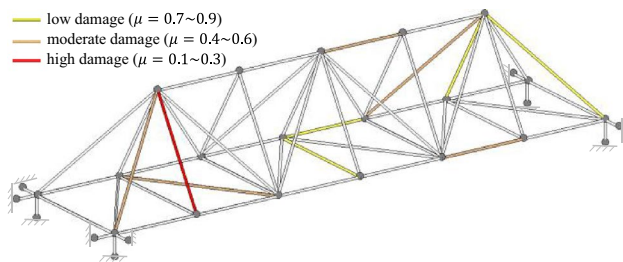
5.2 Truss structure

5.2.1 Truss model

The numerical simulation model of the truss structure is shown in Fig. 13a, in which the number of each member is explicitly shown. The structure is simply supported at both ends, with a length of 2.4 m, a height of 0.45 m, and a width of 0.56 m. There are 51 members and 102 elements in total. The cross-section of each member is shown in Fig. 13b. The outer diameter of the member is 10 mm, and the inner

Table 5 Relative error of the damage factor of the 2nd substructure after every iteration

Method	The relative error at each iteration					
	1st (%)	2nd (%)	3rd (%)	4th (%)	5th (%)	6th (%)
μ_{ω}	54.28	20.35	3.45	1.68	1.70	1.70
μ_m	89.10	15.25	1.43	1.88	1.83	1.83
Mean value of μ	16.26	0.71	0.41	0.38	0.38	0.38

**Fig. 13** Truss structure: **a** 3D truss model, **b** Cross-section shape**Fig. 14** Damage condition of the truss

diameter is 4 mm. The material of the truss structure is steel with Young's modulus of 206 GPa, Poisson ratio of 0.3, and a density of 7850 kg/m³.

It should be emphasized that each member in this model is composed of two beam elements. It allows the excitation to be perpendicularly applied in the middle of each member.

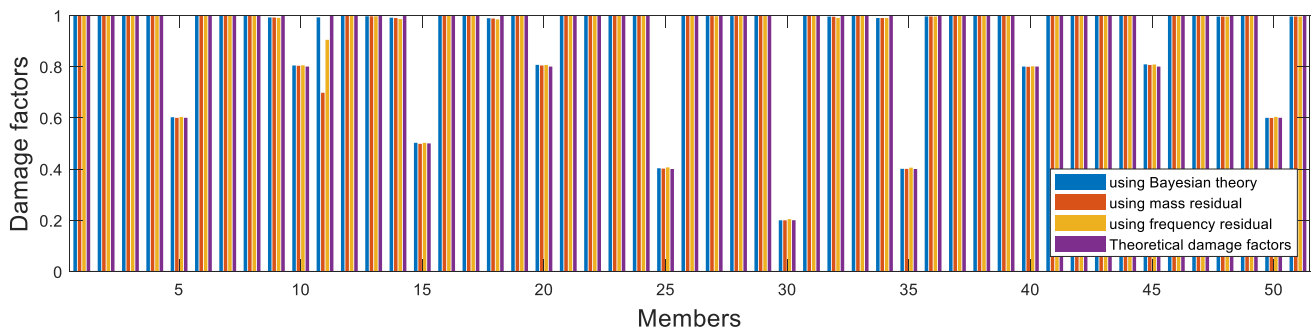
5.2.2 Damage identification

Assume that the damage factors of the damaged truss structure are $\mu(5) = 0.6$, $\mu(10) = 0.8$, $\mu(15) = 0.5$, $\mu(20) = 0.8$, $\mu(25) = 0.4$, $\mu(30) = 0.2$, $\mu(35) = 0.4$, $\mu(40) = 0.8$, $\mu(45) = 0.8$, $\mu(50) = 0.6$, $\mu(\text{others}) = 1.0$ as shown in Fig. 14.

Then, a harmonic excitation is applied to each member of the truss. The direction of the excitation is perpendicular to the involved member, and the excitation point is exactly in the middle of the member (an example is shown in Fig. 13a for member 46). 5% white noises are added to the excitation and the response at the same time.

The first natural frequency is selected to perform damage detection. Based on the analysis of the truss structure, the target frequency can be selected as 20 Hz. By performing the same process as in Sect. 5.1.5, the damage identification results are computed and shown in Fig. 15.

As seen in Fig. 15, damage conditions of all members can be identified. The proposed method using Bayesian theory has a higher precision of damage identification. For example, both deterministic methods wrongly identify member 11 as

**Fig. 15** Damage identification results for the truss structure

a damaged member. It is probably because other members around it are damaged as well (members 10, 45, and 50). However, the proposed method using Bayesian theory can correctly identify it as an intact member.

5.3 3D building

5.3.1 Building model

In this section, a numerical 3D building is designed to verify the proposed method. All 27 components (green for 3 slabs, yellow for 12 beams, and blue for 12 columns) are labeled as in Fig. 16a. Each floor's height is 3.25 m. The cross-section

of the building's columns is $0.25 \times 0.25 \text{ m}^2$, and the cross-section of its beams is $0.25 \times 0.33 \text{ m}^2$. The thickness of 3 slabs is 0.08 m. Both length and width of the slabs are 2.50 m. According to the above parameters, the building is designed with 9.75 m height, 3 m length, and 3 m width.

The material of the building is concrete with Young's modulus of 30 GPa, Poisson ratio of 0.24, and a density of 1950 kg/m^3 . The concrete is simulated by the SOLID 65 element in ANSYS. Each element has 8 nodes, and each node has 3 DOFs that are x, y, z translations. There are 708 elements, 1822 nodes, and 5466 DOFs in total as shown in Fig. 16b. Each component labeled in Fig. 16a is treated as a substructure with the same label. The bottom of the 4 columns (16 nodes) in the first floor is fixed.

5.3.2 Damage identification

In the simulation, harmonic excitations, similar to Eq. (27), are applied perpendicularly at the middle of each substructure. For slabs, the excitation is exactly at the central point. The example excitations are shown in Fig. 16b by red arrows. In the excitation and the response, 5% white noises are added to simulate real-world problems. The damage factors are assumed as $\mu(1) = 0.8$, $\mu(6) = 0.5$, $\mu(9) = 0.3$, $\mu(12) = 0.7$, $\mu(16) = 0.4$, $\mu(18) = 0.1$, $\mu(22) = 0.9$, $\mu(26) = 0.6$, $\mu(27) = 0.2$, $\mu(\text{others}) = 1.0$. The damaged substructures include columns, beams, and slabs to make the simulation closer to real-world scenarios.

The first 3 natural frequencies of the damaged structure can be calculated as 4.0730 Hz, 5.1450 Hz, and 10.7662 Hz. The target frequency is selected as 3.0 Hz after an analysis discussed in Sect. 5.1.3. All estimated masses are utilized in the proposed iterative equations Eq. (16), Eq. (17), and Eq. (24). The mean value of μ using Bayesian theory, μ_m and μ_w can be obtained as shown in Fig. 17.

Figure 17 confirms that all damaged substructures can be identified with an acceptable precision. But for some substructures, the proposed Bayesian approach improves the precision of damage identification (such as substructures 5,

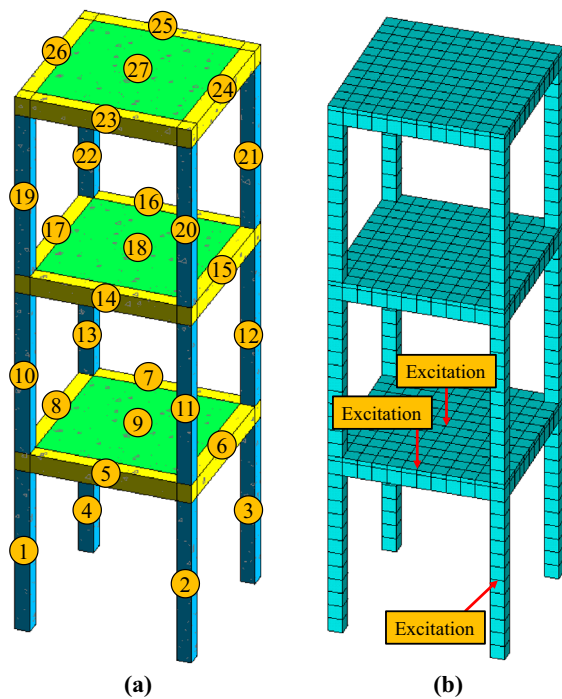


Fig. 16 3D Building and its FE model: **a** Building components (substructures), **b** FE model

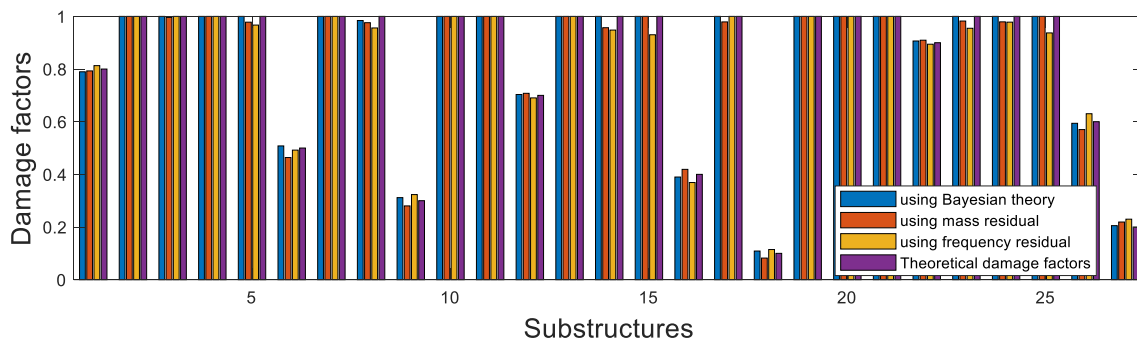


Fig. 17 Damage identification results of the building

8, 9, 14, 15, 16, 23, 24, 25, 26, 27). This shows that the proposed methods can have good applications in practical engineering.

6 Experiment of plane frame structure

6.1 Plane frame structure

As shown in Fig. 18, this section uses a 3-story frame to verify the proposed damage identification method.

The frame height is 0.3 m, the width is 0.295 m, the section height is 0.005 m, and the section width is 0.06 m. Young's modulus of the material is 1.94 GPa and the density is 7850 kg/m³. The frame is divided into 9 substructures, which are numbered as shown in Fig. 18. The

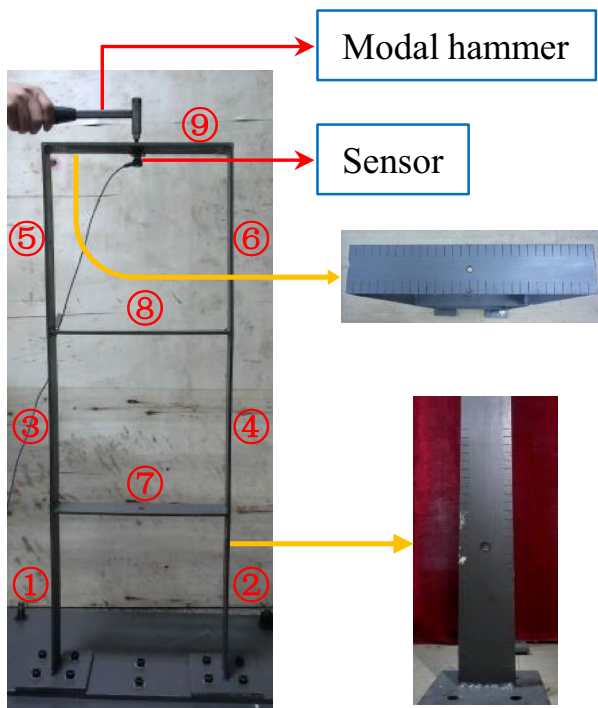
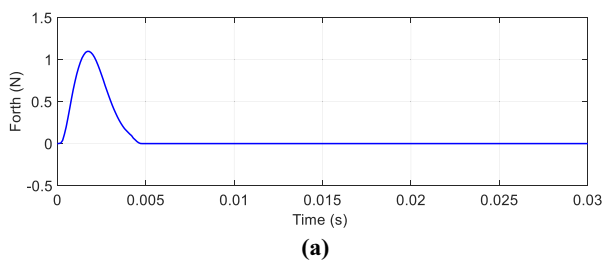


Fig. 18 Experimental model



notches shown in Fig. 18 are cut on the 2nd and the 9th substructure to simulate the damage by reducing the stiffness without affecting the mass. The theoretical damage factor is $\mu = [1, 0.71, 1, 1, 1, 1, 1, 1, 0.54]$. A modal hammer is used to excite the frame, and the excitation time history is recorded. An acceleration sensor is installed at the position of the excitation to measure the response, as required by the proposed method.

6.2 Bayesian damage identification based on virtual mass estimation

In the experiment, the excitation is applied five times, successively to each substructure, and the corresponding responses of the substructure are obtained at the excitation point. In each test, the hammer strike is required to be applied vertically at the position of the sensor, and during the excitation process, multiple strikes must be avoided. The sampling frequency is 10 kHz. Taking the first test for the first substructure as an example, the time-domain excitation and the corresponding response are shown in Fig. 19. The FFT is then applied to determine the acceleration FRF shown in Fig. 20.

Different target frequencies are selected for each substructure and listed in Table 6 ("Target Frequency"). They are determined using frequency reduction factors as discussed by Hou et al. (2020). Besides the target frequencies, Table 6 lists the respective additional virtual masses estimated using Eq. (3) for each of the nine substructures in each of the five tests.

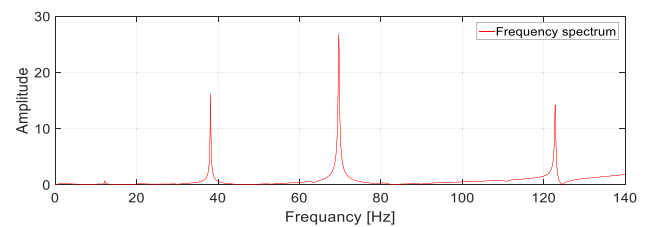


Fig. 20 Acceleration FRF of substructure 1 of the experimental frame

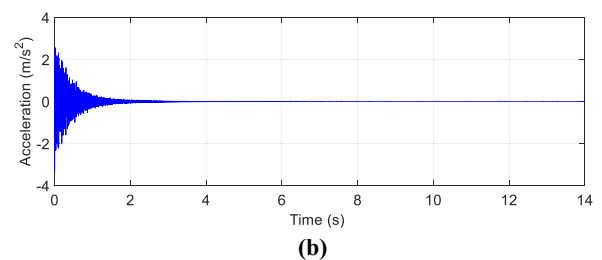


Fig. 19 Excitation and response of substructure 1 of the experimental frame: **a** excitation, **b** acceleration response

Table 6 Target frequencies and the additional virtual masses estimated for each substructure in the five performed tests

Substructure	Target frequency (Hz)	Estimated additional virtual mass (kg)				
		1	2	3	4	5
1	100	2.1239	2.1598	2.1460	2.1448	2.1698
2	110	0.8545	0.9065	0.8952	0.8642	0.8826
3	90	2.3836	2.6984	2.5809	2.8943	2.7097
4	90	2.0485	2.3208	2.3656	2.3413	2.3550
5	90	1.7115	1.7202	1.7046	1.731	1.6766
6	90	1.5888	1.6077	1.5914	1.5971	1.5960
7	93	1.0892	1.0930	1.1053	1.0893	1.1507
8	87	1.0656	1.3665	1.2940	1.3149	1.2580
9	97	0.3315	0.3618	0.3415	0.3439	0.3612

The initial damage factors in the optimization process correspond to the intact structure, $\mu_0 = [1, 1, 1, 1, 1, 1, 1, 1, 1]$. The target frequencies listed in Table 6 are employed in the optimization process using the three methods described in this paper. The results are listed in Table 7. As in the numerical example and Table 3, μ_ω denotes the damage factors identified using the frequency-based objective function Eq. (4), μ_m denotes the results obtained with the proposed mass-based objective function Eq. (5), while the mean values and the standard deviations of the damage factors obtained with the Bayesian approach are listed as “Mean value of μ ” and “Standard deviation of μ .” Additionally, these results are compared with two results obtained earlier in the literature using two variants of the frequency-based approach; they are denoted in Table 7 by μ'_ω (deterministic approach) and μ' (frequency-based Bayesian approach).

Table 7 confirms that both the frequency residual and the mass residual can be used as an objective function to properly identify structural damage. The identification error in both cases is well within 4%. The results obtained using the mass-based Bayesian approach proposed here are similar to the results obtained using an earlier frequency-based Bayesian damage identification. The identified standard deviations of the damage factors are different, but small in both cases.

The error between the mean value and the theoretical value of the damage factor is also well within 4%, which meets the engineering needs.

7 Conclusion

The additional virtual mass method is used to obtain the response of a structure as if an additional mass was physically installed. It can be applied to increase the amount of available modal information, improve structural sensitivity to damage, and decrease the influence of unknown damping. However, its existing versions were based on natural frequencies, had relatively low computational efficiency, and could be influenced by measurement noise.

In this paper, a new objective function based on the residual of estimated masses is proposed, and an iterative identification approach is derived using the Bayesian framework in order to accelerate optimization and improve the identification accuracy.

Numerical simulations of a simply supported beam, a 3D truss structure, and a 3D building model show that the proposed method can accurately and efficiently identify the position and the degree of damages. The method developed

Table 7 Damage identification results (experimental verification)

Substructure	1	2	3	4	5	6	7	8	9
Theoretical value	1.0000	0.7100	1.0000	1.0000	1.0000	1.0000	1.0000	1.0000	0.5400
μ_ω	1.0000	0.6852	0.9923	0.9755	1.0000	1.0000	1.0000	1.0000	0.5103
μ_m	1.0000	0.6807	0.9607	0.9625	1.0000	0.9828	0.9947	0.9867	0.5118
μ'_ω	1.0000	0.6700	0.9670	0.9500	1.0000	1.0000	0.9760	1.0000	0.4910
Mean value of μ	1.0000	0.6818	0.9656	0.9648	0.9923	0.9726	0.9736	0.9913	0.5261
Standard deviation of μ	0.0082	0.0071	0.0236	0.0217	0.0109	0.0091	0.0131	0.0363	0.0086
Mean value of μ'	1.0000	0.6900	0.9800	0.9600	0.9800	0.9700	1.0000	1.0000	0.5100
Standard deviation of μ'	0.0067	0.0050	0.0091	0.0057	0.0067	0.0059	0.0062	0.0060	0.0065

μ'_ω is calculated in Fig. 17 (tuned model using m^*) of reference Hou et al. (2020)

The mean value and standard deviation of μ' are calculated in Table 6 of reference Hou et al. (2018)

using the Bayesian theory is the most accurate and time efficient. The lab frame structure verifies the effectiveness and practical applicability of the method in an experimental scenario.

The research is ongoing to extend the analysis to fully continuous structures, which can further improve the identification accuracy, and to include various models of structural damage.

Acknowledgements The authors gratefully acknowledge the support of the National Natural Science Foundation of China (NSFC) (51878118), the Fundamental Research Funds for the Central Universities (DUT19LK11), and the National Science Centre, Poland (project 2018/31/B/ST8/03152).

Declarations

Conflict of interest The authors declare no conflict of interest. We would like to declare that the work described was original research that has not been published previously and not under consideration for publication elsewhere, in whole or in part.

Replication of results Data are available from authors upon request.

References

- Adhikari S (2006) Damping modelling using generalized proportional damping. *J Sound Vib* 293:156–170
- Adhikari S, Woodhouse J (2001) Identification of damping: part 1, viscous damping. *J Sound Vib* 243:43–61
- Astroza R, Nguyen LT, Nestorović T (2016) Finite element model updating using simulated annealing hybridized with unscented Kalman filter. *Comput Struct* 177:176–191. <https://doi.org/10.1016/j.compstruc.2016.09.001>
- Bagheri A, Ozbulut OE, Harris DK (2018) Structural system identification based on variational mode decomposition. *J Sound Vib* 417:182–197. <https://doi.org/10.1016/j.jsv.2017.12.014>
- Bayissa WL, Haritos N, Thelandersson S (2008) Vibration-based structural damage identification using wavelet transform. *Mech Syst Signal Process* 22:1194–1215. <https://doi.org/10.1016/j.ymssp.2007.11.001>
- Beck JL, Papadimitriou C, Au S-K, Vanik MW (1998) Entropy-based optimal sensor location for structural damage detection. In: *Smart Structures and Materials 1998: Smart Systems for Bridges, Structures, and Highways*. International Society for Optics and Photonics, pp 161–172
- Chang K-C, Kim C-W (2016) Modal-parameter identification and vibration-based damage detection of a damaged steel truss bridge. *Eng Struct* 122:156–173. <https://doi.org/10.1016/j.engstruct.2016.04.057>
- Dackermann U, Li J, Samali B (2011) Identification of added mass on a two-storey framed structure utilising FRFs and ANNs
- Dems K, Mróz Z (2010) Damage identification using modal, static and thermographic analysis with additional control parameters. *Comput Struct* 88:1254–1264
- Dolatabadi PD, Khanlari K, Ghafory Ashtiany M, Hosseini M (2020) System identification method by using inverse solution of equations of motion in time domain and noisy condition. *Phys A Stat Mech Its Appl*. <https://doi.org/10.1016/j.physa.2019.122680>
- Dragomiretskiy K, Zosso D (2014) Variational mode decomposition. *IEEE Trans Signal Process* 62:531–544. <https://doi.org/10.1109/tsp.2013.2288675>
- Gillich GR, Furdui H, Abdel Wahab M, Korka ZI (2019) A robust damage detection method based on multi-modal analysis in variable temperature conditions. *Mech Syst Signal Process* 115:361–379. <https://doi.org/10.1016/j.ymssp.2018.05.037>
- Hoskere V, Eick B, Spencer BF et al (2019) Deep Bayesian neural networks for damage quantification in miter gates of navigation locks. *Struct Heal Monit*. <https://doi.org/10.1177/1475921719882086>
- Hou J, An Y, Wang S et al (2018) Structural damage localization and quantification based on additional virtual masses and Bayesian theory. *J Eng Mech*. [https://doi.org/10.1061/\(ASCE\)EM.1943-7889.0001523](https://doi.org/10.1061/(ASCE)EM.1943-7889.0001523)
- Hou J, Jankowski L, Ou J (2013) Structural damage identification by adding virtual masses. *Struct Multidiscip Optim* 48:59–72. <https://doi.org/10.1007/s00158-012-0879-0>
- Hou J, Li Z, Jankowski L, Wang S (2020) Estimation of virtual masses for structural damage identification. *Struct Control Heal Monit*. <https://doi.org/10.1002/stc.2585>
- Huang Y, Li H, Wu S, Yang Y (2018) Fractal dimension based damage identification incorporating multi-task sparse Bayesian learning. *Smart Mater Struct*. <https://doi.org/10.1088/1361-665X/aac248>
- Jayalakshmi V, Rao ARM (2017) Simultaneous identification of damage and input dynamic force on the structure for structural health monitoring. *Struct Multidiscip Optim* 55:2211–2238. <https://doi.org/10.1007/s00158-016-1637-5>
- Khatir S, Abdel Wahab M (2019) Fast simulations for solving fracture mechanics inverse problems using POD-RBF XIGA and Jaya algorithm. *Eng Fract Mech* 205:285–300. <https://doi.org/10.1016/j.engfracmech.2018.09.032>
- Khatir S, Abdel Wahab M, Boutchicha D, Khatir T (2019) Structural health monitoring using modal strain energy damage indicator coupled with teaching-learning-based optimization algorithm and isogeometric analysis. *J Sound Vib* 448:230–246. <https://doi.org/10.1016/j.jsv.2019.02.017>
- Khatir S, Boutchicha D, Le Thanh C et al (2020) Improved ANN technique combined with Jaya algorithm for crack identification in plates using XIGA and experimental analysis. *Theor Appl Fract Mech* 107:102554. <https://doi.org/10.1016/j.tafmec.2020.102554>
- Kim JT, Ryu YS, Cho HM, Stubbs N (2003) Damage identification in beam-type structures: frequency-based method vs mode-shape-based method. *Eng Struct* 25:57–67. [https://doi.org/10.1016/s0141-0296\(02\)00118-9](https://doi.org/10.1016/s0141-0296(02)00118-9)
- Kořakowski P, Wikło M, Holnicki-Szulc J (2008) The virtual distortion method—a versatile reanalysis tool for structures and systems. *Struct Multidiscip Optim* 36:217–234
- Law SS, Lin JF (2014) Unit impulse response estimation for structural damage detection under planar multiple excitations. *J Appl Mech Trans ASME*. <https://doi.org/10.1115/1.4025320>
- Lazhari M, Sadhu A (2019) Decentralized modal identification of structures using an adaptive empirical mode decomposition method. *J Sound Vib* 447:20–41. <https://doi.org/10.1016/j.jsv.2019.01.049>
- Lee U, Shin J (2002a) A frequency-domain method of structural damage identification formulated from the dynamic stiffness equation of motion. *J Sound Vib* 257:615–634
- Lee U, Shin J (2002b) A frequency response function-based structural damage identification method. *Comput Struct* 80:117–132. [https://doi.org/10.1016/s0045-7949\(01\)00170-5](https://doi.org/10.1016/s0045-7949(01)00170-5)
- Li J, Law SS, Ding Y (2012) Substructure damage identification based on response reconstruction in frequency domain and model updating. *Eng Struct* 41:270–284. <https://doi.org/10.1016/j.engstruct.2012.03.035>

- Lin S-W, Yi T-H, Li H-N, Ren L (2017) Damage detection in the cable structures of a bridge using the virtual distortion method. *J Bridge Eng* 22:4017039
- Lu P, Wang L, Duan J et al (2017) Influencing factors of beam structure damage identification based on additional mass. *J PLA Univ Sci Technol (natural Sci Ed)* 18:295–301
- Moughy JJ, Casas JR (2018) Damage identification of bridge structures using the Hilbert-Huang transform. In: *Life cycle analysis and assessment in civil engineering: towards an integrated vision: proceedings of the sixth international symposium on life-cycle civil engineering (IALCCE 2018)*, pp 28–31
- Mousavi M, Holloway D, Olivier JC (2020) A new signal reconstruction for damage detection on a simply supported beam subjected to a moving mass. *J Civ Struct Heal Monit* 10:709–728. <https://doi.org/10.1007/s13349-020-00414-3>
- Nalittlela N, Penny JET, Friswell MI (1993) Updating model parameters by adding an imagined stiffness to the structure. *Mech Syst Signal Process* 7:161–172. <https://doi.org/10.1006/mssp.1993.1005>
- Rajendran P, Srinivasan SM (2015) Performance of rotational mode based indices in identification of added mass in beams. *Struct Eng Mech* 54:711–723
- Salawu OS (1997) Detection of structural damage through changes in frequency: a review. *Eng Struct* 19:718–723
- Sedehi O, Papadimitriou C, Katafygiotis LS (2019) Probabilistic hierarchical Bayesian framework for time-domain model updating and robust predictions. *Mech Syst Signal Process* 123:648–673. <https://doi.org/10.1016/j.ymssp.2018.09.041>
- Spanos NA, Sakellariou JS, Fassois SD (2020) Vibration-response-only statistical time series structural health monitoring methods: a comprehensive assessment via a scale jacket structure. *Struct Heal Monit* 19:736–750. <https://doi.org/10.1177/1475921719862487>
- Suwała G, Jankowski Ł (2012) A model-free method for identification of mass modifications. *Struct Control Heal Monit* 19:216–230
- Tang T, Zhu Y, Cai D, Liu H (2006) Virtual flexibility matrix on structural crack damage detection. *J Sichuan Univ Eng Sci Ed* 38:39–42
- Yan G, Sun H, Waisman H (2015) A guided Bayesian inference approach for detection of multiple flaws in structures using the extended finite element method. *Comput Struct* 152:27–44
- Zhang D, Li S, Li H (2019) Adaptive substructure identification for shear structures with virtual control system. *Mech Syst Signal Process* 121:426–440
- Zhang D, Yang Y, Wang T, Li H (2018) Improving substructure identification accuracy of shear structures using virtual control system. *Smart Mater Struct*. <https://doi.org/10.1088/1361-665X/aaa46f>
- Zhang J, Aoki T (2020) A frequency-domain noniterative algorithm for structural parameter identification of shear buildings subjected to frequent earthquakes. *Comput Civ Infrastruct Eng* 35:615–627
- Zhang Q, Hou J, Jankowski Ł (2020) Bridge damage identification using vehicle bump based on additional virtual masses. *Sensors (switzerland)*. <https://doi.org/10.3390/s20020394>
- Zhang Q, Jankowski Ł (2017) Damage identification using structural modes based on substructure virtual distortion method. *Adv Struct Eng* 20:257–271

Publisher's Note Springer Nature remains neutral with regard to jurisdictional claims in published maps and institutional affiliations.